Query Details

1. Please confirm if the author names are presented accurately and in the correct sequence (given name, middle name/initial, family name).

Yes, they are

2. Please confirm if the processed affiliation 1 and 3 are correct.

Aff1 is correct.

See correction on Aff3

3. Please check and confirm the inserted journal name, page, issue, volume number in the reference 26 is correct.

Reference 26 was corrected

4. Please check and confirm the inserted journal name, published yaer in the reference 27 is correct.

Reference 27 was corrected

5. Please check and confirm the inserted journal name in the reference 21 is correct.

Reference 21 was corrected

Original Papers

Determination of association equilibrium constant from single molecule fluorescence localization microscopy

M. Victoria Cappellari   Affiliationids : Aff1

Luis F. Marcano-García   Affiliationids : Aff1

Sabrina Simoncelli   Affiliationids : Aff2

Pedro F. Aramendía ✉

Email : pedro.aramendia@cibion.conicet.gov.ar

Affiliationids : Aff1 Aff3, Correspondingaffiliationid : Aff1

Aff1 Centro de Investigaciones en Bionanociencias -‘‘Elizabeth Jares-Erijman’’ (CIBION), CONICET, Godoy Cruz 2390, 1425, Ciudad de Buenos Aires, Argentina

Aff2 London Centre for Nanotechnology and Department of Chemistry, University College London, London, WC1H 0AH, UK

Aff3 ~~Departamento de Química Inorgánica, Analítica Y Química Física. Facultad de Ciencias Exactas Y Naturales~~ Departamento de Química Inorgánica, Analítica y Química Física. Facultad de Ciencias Exactas Y Naturales, Universidad de Buenos Aires, 1428, Ciudad de Buenos Aires, Argentina

Abstract

Single molecule fluorescence localization microscopy provides molecular localization with a precision in the tens of nanometer range in the plane perpendicular to the light propagation. **AQ1** This opens the possibility to count molecules and correlate their locations, starting from a map of the actual positions in a single molecule super resolution image. Considering molecular pair correlation as an indication of interaction, and a way to discern them from free molecules, we describe a method to calculate thermodynamic equilibrium constants. **AQ2** In this work, we use as a test system two complementary *homo*-oligonucleotides, one strand marked with Cyanine 3.5 and the other with Alexa Fluor 647. Hybridization is controlled by the amount of each strand, temperature, and the ionic force, and measured in steady state emission. The same samples are examined in Stochastic Optical

labelling-detection efficiency, and determination of the critical distance for association are discussed. We consistently determine values in STORM coincident with those of the bulk experiment.

Graphical abstract
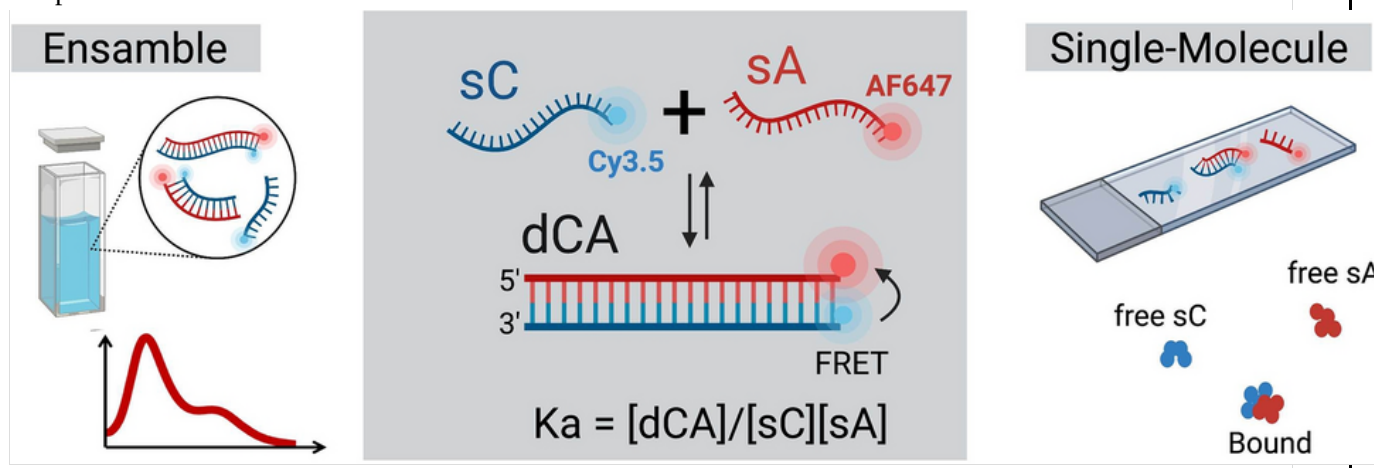
Keywords

Super resolution
Fluorescence
Hybridization
Equilibrium constant
FRET

Supplementary Information

The online version contains supplementary material available at https://doi.org/10.1007/s43630-022-00254-8.

---

1. **Introduction**

Single molecule localization microscopy (SMLM) allows to optically map molecular positions with a routine localization precision of 10–40 nm [1, 2, 3, 4, 5] opening up the possibility to determine molecular spatial correlation with unprecedented detail compared to the hundreds of nm of conventional confocal microscopy [6, 7, 8]. Still, as the typical molecular size of common organic molecules lies in the 1–2 nm range and proteins extend to 3–10 nm, the precision achieved in localization is not a direct demonstration of molecular proximity in the range of strong molecular interactions and thus, we remain in the statistical domain of correlation of positions [7, 9, 10, 11]. Compared to confocal microscopy, however, SMLM provides a comparative advantage as its quantitative aspect enables to count free and bound molecular species which can render a numerical parameter to evaluate the strength of the association. Even further, compared to other experimental methods used to study association (constants) in biological systems, SMLM has the advantage that the parameter of the interaction could, in principle, be determined in their physiological environment, for example, in a cell cytoplasm, membrane or organelle [10, 12, 13, 14].

The reward seems interesting provided we can successfully tackle phenomena inherent to quantitative SMLM. The first factor that must be taken into consideration is the multiple location of the same molecule, due to multiblinking or extended ON cycles [15]. This results in clustered locations, which in principle can be attributed to various determinations of the position of the same molecule within location uncertainty, or to various molecules of the same species aggregated in a space smaller than the localization uncertainty. The second factor arises in the incomplete labelling (because of incomplete reaction of the biomolecule with the fluorophore or incomplete labelling efficiency of antibodies against the proteins of interest) and detection steps that results in undercounting individual molecules, or, in the case of associated pairs, their consideration as lonely molecules if one of the partners is undetected for some reason (bleaching or orientation effects) [16, 17]. Also, and because of the change in the number of moles in an association process, the volume in which molecules are counted is an important factor to convert ratio of numbers of molecules into an association (or dissociation) thermodynamic equilibrium constant. Finally, an interaction radius for the consideration of association has to be defined. Statistically, this distance must be related to the mean uncertainty in the determination of molecular position [18].

In this paper, we undertake comparative measurements of hybridization of complementary DNA sequences in solution and in Stochastic Optical Reconstruction Microscopy (STORM) of spin coated poly(vinylalcohol) (PVA) films of these same solutions. In standard bulk solution experiments, association is evaluated by fluorescence spectroscopy. In STORM experiments, we use spatial statistical methods to account for multiblinking. Furthermore, mass balance analysis of incomplete labelling-detection demonstrates that extrapolation to infinite dilution results in the most trustful value of the equilibrium constant. The comparison of the results of both sets of experiments provides a reference to ascertain the feasibility and conditions under which a relevant value for the equilibrium constant can be obtained from SMLM experiments. We discuss the limitations of the method and the concentration range in which it can be practically applicable.

2. **Materials and methods**

Oligonucleotides, purified by HPLC, were purchased from Eurofins Genomics. PolyA and PolyT, 20 bp, labelled with Cyanine 3.5 at 5' end (PA-Cy3.5-5'), and Alexa Fluor 647 at 3' end (PT-AF-3'), respectively, were custom synthesized. For comparison purposes, PolyA and PolyT, 20 bp, without labels were also used. Fresh strands were resuspended in TAE12 10 mM, aliquoted and stored at – 20 ℃ for further use. Mowiol Merck (MW:31,000) 1% w/v solution in TAE12 was used for spin coating (see below).

2.2. Spectroscopy

The concentration of the polynucleotide solutions was determined by absorption spectroscopy on a Shimadzu UV-3600, using the absorption coefficient at 260 nm informed by the manufacturer. Steady state fluorescence experiments were performed on a PTI QM40 spectrofluorometer. Emission was corrected for the spectral sensitivity of the detection channel. Samples, contained in a 1 cm square quartz cuvette with a Teflon stopper, were excited at 550 nm and 604 nm. The cuvette temperature was controlled at 25 ℃ with a Peltier element.

2.3. Super-resolution fluorescence microscopy STORM imaging

A custom-built microscope was used, based on a 642 nm, 5 mW laser (MPB Communications 2RU-VFL-P-1500-642) for fluorescence excitation of Alexa Fluor 647, and a 532 nm 5 mW laser (Laser Quantum Ventus 532) for fluorescence excitation of Cyanine 3.5. The lasers were combined with dichroic mirrors (Semrock LM01-427 and LM01-552), magnified, and then focused onto the back focal plane of an oil immersion objective Olympus PlanApo 60 × NA 1.42. A dichroic mirror (Semrock Di03-R 405/488/532/635-t1) and a band-pass filter (Chroma ET700/75 m) were used for decoupling the fluorescence emission of the sample from the laser excitation. Further blocking of the excitation laser light was performed with a multiedge notch filter (Semrock NF03-405/488/532/635E). The emission light was expanded with a 2 × telescope so that the pixel size of the EMCCD camera (Andor iXon3 897) would match the optimal value for single-molecule localization, 133 nm per pixel in the focal plane. Finally, fluorescent emission from different species were separated with a dichroic mirror (Chroma ZT647rdc) and imaged onto adjacent areas of the camera. Differences in magnification, shear, and image rotation between the two channels were considered to obtain an accurate overlay of the final reconstructed images. This is achieved by imaging isolated fluorescent markers visible on both channels (Life Technologies Tetraspeck 0.1 µm) and then finding the affine transformation that minimizes the distance between the same markers as detected in each detection channel.

2.4. Sample preparation

Oligonucleotide solutions of equal molar amounts of each component were allowed to hybridize for 1 h and then brought to final concentration in Mowiol 1% in TAE12. After that, 50 µL of the solutions were spin coated (Laurell Inc.) at 3000 rpm during 45 s onto plasma-clean 22 × 22 mm #1.5 Menzel Gläser coverslips. Finally, samples were dried under vacuum for 2 h at 40 ℃ and imaged in the microscope within the same day of preparation.

2.5. Atomic force microscopy (afm)

Topographic imaging by AFM was acquired in tapping mode using silicon tips with a spring constant of 42 N m^{-1} and a resonance frequency of 320 kHz. The equipment was a Bruker Multimode 8SPM (Santa Barbara, CMA, USA) and a NanoScope V Controller (Santa Barbara, CMA, USA). A neat step in the polymer film was produced by cutting with a scalpel and removing one side. The height of the polymer step was measured by triplicate in different polymer regions.

3. Results

3.1. Steady state emission in bulk experiments

We performed hybridization experiments with each of the oligonucleotides in the 5–200 nM concentration range. In each set of experiments, one component is in excess at a constant total concentration, while the other is added in increasing proportions to control the degree of hybridization. PolyA-Cy3.5-5' (PA-Cy3.5-5') was excited at 550 nm, while PolyT-Alexa Fluor647-3' (PT-AF-3') was excited at 604 nm. In the mentioned concentration range, absorbance at the excitation wavelength is less than 0.05. This upper limit assures that the fraction of light absorbed by each fluorophore as well as the total fraction absorbed are in the linear regime with concentration. Consequently, the amount of light absorbed by PA-Cy3.5-5' is not influenced by the small amount of light absorbed at 550 nm by the addition of PT-AF-3'. The assumption is that the absorption coefficient of the fluorophore is the same in the single and in the double stranded DNA. We performed hybridization experiments of PA-Cy3.5-5' with PT-AF-3', PA-Cy3.5-5' with PolyT (PT, without fluorophore), and of PT-AF-3' with PolyA (PA, also without fluorophore).

Figure 1 shows the emission spectra of PA-Cy3.5-5' (solid green line), PA-Cy3.5-5'—PT-AF-3' (dashed blue line) and PA-Cy3.5-5'—PT (dotted red line) mixtures all at 100 nM concentration for each component and excited at 550 nm. Under these conditions, the emission of PT-AF-3' is negligible. There is a small deactivation of Cy3.5 emission by hybridization, in line with previous reports characterizing the fluorescence quenching of nucleotides [19]. Deactivation is much higher upon hybridization with PT-AF-3' that provides a FRET pathway. Besides this evidence, the capability of Cy3.5 (donor) and AlexaFluo647 (acceptor) to act as a FRET pair was also demonstrated in the literature by measurement of the fluorescence lifetime shortening of Cy3.5 from 1.6 ns when isolated, to ca. 0.6 ns in the presence of AlexaFluor647 [20].

Fig. 1

Emission spectra of 100 nM PA-Cy3.5-5' (solid green line), and of an equilibrated PA-Cy3.5-5'**—**PT (dotted red line) and PA-Cy3.5-5'**—**PT-AF-3' (dashed blue line) mixture, 100 nM in each component. The samples were excited at 550 nm

Figure 2 displays the normalized change in emission intensity of 100 nM PA-Cy3.5-5', $\Delta I_f = (I_f - I_0)/I_0$, as a function of added fraction of complementary strand, being it PT-AF-3' (blue triangles) or PT (red circles). It also displays the values of ΔI_f when PA is added to 100 nM PT-AF-3' (black squares). In this later case, we monitored the emission of Alexa Fluor at 665 nm.

Fig. 2

A Emission spectra of equilibrated mixtures of PA-Cy3.5-5' with PT-AF-3'. Percentages in the inset are 100. [PT-AF-3']/[PA-Cy3.5-5']. **B** Ratio $(I - I_0)/I_0$ vs. percentage of the added component for hybridization of 100 nM PT-AF-3' by adding PA (black squares); 100 nM PA-Cy3.5-5' by adding PT (red circles), and of 100 nM PA-Cy3.5-5' by adding PT-AF-3'(blue triangles) determined at 602 nm emission wavelength for PA-Cy3.5-5' mixtures, and 665 nm for PT-AF-3' ones. Percent concentration indicates the proportion of added oligonucleotide relative to the initial concentration of the other component

Linear behaviour of these curves implies a complete association of the complementary strands, as will be shown below. This fact is demonstrated in Figure S1, where the hybridization curves of 100 and 200 nM PA-Cy3.5-5' with PT-AF-3' coincide within experimental uncertainty. In consequence, the curve for 100 nM PA-Cy3.5-5' with variable amounts of added PT-AF-3' will serve as

experiments.

In what follows we will develop the equations used to obtain K_h, [19]

$$SS1 + SS2 \Leftrightarrow DS$$

$$K_h = \frac{[DS]}{[SS1] \cdot [SS2]}$$

1

where SS1 and SS2 are the two complementary single stranded oligonucleotides that hybridize to the double stranded, DS, species.

In fluorescence emission experiments, where excitation is performed at 550 nm, and emission is measured at 602 nm, only Cy3.5 contributes appreciably to the emission intensity. On one side, at 550 nm the absorption coefficient of AF is 14000 M^{-1} cm^{-1}, compared to 87,000 M^{-1} cm^{-1} of Cy3.5. On the other side, in the 4 nm bandwidth around 602 nm, 6% of the emission of Cy3.5 (ϕ_f = 0.15) is collected, compared to less than 0.1% collected for the emission of AF (ϕ_f = 0.33). Furthermore, in these experiments, the sum of Cy3.5 containing species is always in excess compared to the sum of AF containing ones.

Consequently, the only two species contributing to emission under the mentioned conditions are the single stranded PA-Cy3.5-5' and the double stranded PA-Cy3.5-5'—PT-AF-3' or PA-Cy3.5-5'—PT. To simplify notation in the following equations, we will term the single stranded species as: sC for PA-Cy3.5-5'; sA for PT-AF-3', while PA and PT without fluorescent label preserve their symbol. The double stranded species will be termed: dCA for PA-Cy3.5–5'—PT-AF-3'; dC0 for PA-Cy3.5–5'—PT; and dA0 for PT-AF-3'—PA.

In PA-Cy3.5–5'—PT-AF-3' hybridization experiments, mass conservation for the total amount of single strands, sC and sA, indicates that:

$$[sC]_t = [sC] + [dCA]$$

$$[sA]_t = [sA] + [dCA]$$

2

If we assume that Cy3.5 displays equal absorption coefficient in the double stranded as in the single stranded species, then the total emission intensity at 602 nm will be:

3

$$I_f = \kappa \epsilon_C \left(\phi_{f,C}^{sC} \cdot [sC]_t + \left(\phi_{f,C}^{dCA} - \phi_{f,C}^{sC} \right) \cdot [dCA] \right)$$

where κ is a proportionality constant and $\phi_{f,C}^{sC}$, $\phi_{f,C}^{dCA}$, are the emission quantum yields of Cy3.5 in sC and in dCA, respectively.

The first term in Eq. 3 corresponds to the emission intensity of the total initial concentration, that we will call I_0. To normalize experimental results, we use ΔI_f, defined before:

4

$$\Delta I_f = \frac{I_f - I_0}{I_0} = \frac{\phi_{f,C}^{dCA} - \phi_{f,C}^{sC}}{\phi_{f,C}^{sC}} \cdot \frac{[dCA]}{[sC]_t}$$

At 100 nM initial concentration of sC, and in excess of this oligonucleotide compare to sA, we can consider that all added sA is hybridized, and consequently negligible amounts of sA free are left in solutions, therefore $[sA]_t = [dCA]$, from Eq. 2. In this case, ΔI_f, assumes the value for the complete reaction, $\Delta I_{f,CR}$

5

$$\Delta I_{f,CR} = \frac{I_f - I_0}{I_0} = \frac{\phi_{f,C}^{dCA} - \phi_{f,C}^{sC}}{\phi_{f,C}^{sC}} \cdot \frac{[sA]_t}{[sC]_t}$$

Equation 5 expresses the fact that, provided association is complete, the representation of ΔI_f vs. the ratio of total concentration of each component should be a straight line, only dependent on the difference in emission quantum yields and relative concentration: $[sA]_t/[sC]_t$.

The linear behaviour shown in Fig. 2 points to a complete hybridization in the conversion interval and at 100 nM concentration (see also Figure S1). Therefore, this curve, registered at 100 nM, serves as reference for what is expected under complete association at any total concentration. This holds because in the concentration range of the experiments free quencher in solution cannot afford appreciable deactivation considering that the diffusion time (in the milliseconds range) is much longer than the excited state lifetime of Cy3.5 in the subnanosecond range [21].

At lower concentrations of initial sC, plots show a lower relative decrease in the emission intensity as a consequence of partial hybridization. The fraction of associated strands can be determined from the ratio in Eqs. 4 and 5, provided the value in Eq. 5 is computed at 100 nM total concentration and at the same $[sA]_t/[sC]_t$. Then, knowing [dCA], $[sA]_t$, and $[sC]_t$, all concentrations can be calculated to compute:

$$K_h = \frac{[dCA]}{[sC] \cdot [sA]}$$

6

Figure 3A displays ΔI_f as a function of relative concentration for 10, 50, and 100 nM PA-Cy3.5–5'—PT-AF-3' experiments. Following the procedure described above, K_h was calculated for the two lower concentrations, as plotted in Fig. 3B.

Fig. 3

A ΔI_f as a function of relative concentration $[sA]_t/[sC]_t$ for hybridization of PA-Cy3.5-5' with PT-AF-3' at different initial concentration of PA-Cy3.5-5'. **B** Log K_h, calculated as described in the text for each point

The average value is $\log(K_h/M^{-1}) = 8.0 \pm 0.3$, in agreement with literature values for similar strands and hybridization conditions [22, 23, 24].

3.2. **Single molecule experiments**

We performed STORM experiments on samples prepared by spin coating stoichiometric mixtures of PA-Cy3.5–5'—PT-AF-3' in 1% Mowiol solutions, previously allowed to hybridize for 1 hour in the dark. Excitation was performed simultaneously at 532 and 642 nm to excite both dyes. Emission was detected by a CCD camera in two separate channels to monitor emission from both dyes. Figure 4 shows the locations in each channel after image processing. These raw single-molecule localizations must be processed to obtain K_h starting from the number of molecules of each species, N_i:

$$Q_{CA} = \frac{N_{dCA}}{N_{sC} \cdot N_{sA}}$$

7

Fig. 4

A Render super-resolution image of the total localizations obtained for both channels; blue: Cy3.5 emission and red: AF emission. **B** Center of mass of clusters of single-molecule localisations containing at least 5 points. Blue crosses: Cy3.5 isolated molecules; red crosses: AF isolated molecules; white circles: pairs of Cy3.5 and AF identified as associated. Scale bar in these two panels is 1 μm. **C** Detail of the region in panel b, showing associated and isolated molecules. **D** Complementary cumulative distribution function of the distance to the first neighbour as a function of distance for the distribution of molecules of AF-AF (red circles); Cy3.5-Cy3.5 (blue circles); AF-Cy3.5 (red crosses); Cy3.5-AF (blue crosses)

To transform Q_{CA} into K_h we need to convert the molecular numbers into concentrations, and for that we must know the magnitude of the observation volume, V_{obs}. This is readily calculated by calibrating the field of view in the camera, and the thickness of the polymer film. The field of view is 16×32 μm^2. Spin coating produces homogeneous films of reproducible thickness provided production variables are carefully controlled (polymer concentration, solvent, rotation speed, and acceleration) [25]. The height of the polymer

step was measured by AFM in triplicate in different polymer regions in each of three independent samples resulting in an average thickness of 40 ± 2 nm (see Figure S2). Thus:

$$K_h = Q_{CA} . N_A . V_{obs}$$

<div align="right">8</div>

where $\boxed{N_A}$ corresponds to the Avogadro number.

In turn, the absolute number of single-molecule localizations for single and double stranded DNAs have to be analyzed to take into account (i) multiblinking, which results in computing the same molecule more than once, (ii) incomplete labelling-detection of molecules, which results in undercounting single strands and mistaking double strands by single ones, or undercounting them if both dyes are not detected, and (iii) a critical distance must be established to distinguish associated pairs from isolated single strands.

Multiblinking is evident in the localization image of Fig. 4 A because points appear forming clusters of the same color, whereas these clusters are well separated from each other. A density-based spatial clustering algorithm, known as DBSCAN, was used to identify clusters of single molecules localizations [26, 27, 28]. DBSCAN identifies clusters by searching for a minimum number of points (3 in the present work) within a circle of specified radius (100 nm in the present work). If we replace the locations belonging to each cluster by the cluster's center of mass, we obtain the distributions that are depicted as an example on Fig. 4 B. The center of mass positions are compatible with a random distribution. This fact is shown on Fig. 4 D. The complementary cumulative distribution function of the distance to the first neighbor, CCDF(r), should be linear with the square of the distance, [29, 30] according to

$$\log\,(\mathrm{CCDF}\,(\mathrm{r}))\,=\,-\,\mathrm{a}.\,\mathrm{r}^2.$$

<div align="right">9</div>

Furthermore, if we consider the complete set of single-molecule localizations of Fig. 4 A, a value for Q_{CA} smaller than the one for a random distribution is obtained (see Table S1). This can be explained because in a cluster, only those members near the borders of the cluster can be identified as interacting pairs with other species, whereas those localizations more near the center of the cluster are much farther away. These two facts justify our decision to replace each cluster by its center of mass.

Cluster analysis also renders the distribution of the number of localizations belonging to each cluster as well as the cluster size as measured by the major and minor axes of the ellipsoid that better fits its form. The results are depicted in Figure S3. Most of the clusters are integrated by less than 10 points, and the average size of the major and minor axes are: 150 ± 70 and 70 ± 40 nm for Cy3.5 clusters, and 220 ± 100 and 100 ± 60 nm for AF clusters.

Finally, CCDF(r) shows that first neighbours between Cy3.5 and AF are nearer than for Cy3.5-Cy3.5 or AF-AF pairs, a clear indication of the expected association. This is shown in Fig. 4 D (comparison of crosses vs circles, respectively).

In agreement with the cluster size, we established a critical distance for association of 100 nm for Cy3.5 and AF bright spots. Pairs that fulfil this condition are circled in the example of Fig. 4 B and shown in detail in the enlargement of the region of interest selected in Fig. 4 C, as different from red crosses of AF for sA, and blue crosses of Cy3.5 for sC.

Finally, we analyze quantitatively the effect of detecting only a fraction, f_C and f_A, of the total number of Cy3.5 and AF fluorophores, respectively. The total number of molecules of each species can be expressed by Eqs. 10a , b, c as a function of these detection probabilities, and assuming that these probabilities are the same in the double as in the single strands:

$$N_{sC} = f_C . N_{sC} + (1 - f_C) . N_{sC}$$

<div align="right">10a</div>

$$N_{sA} = f_A . N_{sA} + (1 - f_A) . N_{sA}$$

<div align="right">10b</div>

$$N_{dCA} = f_C . f_A . N_{dCA} + f_C . (1 - f_A) . N_{dCA} + (1 - f_C) . f_A . N_{dCA} + (1 - f_C) . (1 - f_A) . N_{dCA}$$

<div align="right">10c</div>

In Eqs. 10a, b, c, the first term of the second member accounts for those molecules correctly identified. The second term of the second member in Eqs. 10a and 10b represent those undetected molecules. In Eq. 10c , the second term represents the number of double strands counted as lonely Cy3.5 molecules, whereas the third accounts for those computed as AF molecules, and the fourth is the number of undetected double strands because none of the two fluorophores are detected.

The number of molecules identified as belonging to each species (identified with the superscript D) under these assumptions are

$$N_{sC}^D = f_C . N_{sC} + f_C . (1 - f_A) . N_{dCA}$$

<div align="right">11a</div>

$$N_{sA}^D = f_A . N_{sA} + (1 - f_C) . f_A . N_{dCA}$$

<div align="right">11b</div>

$$N_{dCA}^D = f_C . f_A . N_{dCA}$$

<div align="right">11c</div>

In Eqs. 11 a and b, the second term in the second member accounts for double stranded molecules with either of the fluorophores

If we compute the experimental value of Q_{CA}, by using the number of detected molecules, it can be readily related to the actual one using Eqs. 11 a ~~and b~~, b, c.

$$\frac{1}{Q_{CA}^{exp}} = \frac{(f_C . N_{sC} + f_C . (1 - f_A) . N_{dCA}) . (f_A . N_{sA} + (1 - f_C) . f_A . N_{dCA})}{f_C . f_A . N_{dCA}}$$

12

After factorization and rearrangement, Eq. 12 can be written as:

$$\frac{1}{Q_{CA}^{exp}} = \frac{1}{Q_{CA}} + (1 - f_C) . N_{sC} + (1 - f_A) . N_{sA} + (1 - f_C)(1 - f_A) . N_{dCA}$$

13

Equation 13 relates the experimental and the actual value of Q_{CA}. The difference between their inverse values is equal to the total number of undetected molecules of all species. This result indicates that the actual value of Q_{CA} can be obtained from the experimental one by extrapolation to zero concentration.

We computed the experimental Q_{CA} in different portions of various spin coated samples. Figure 5 displays the behaviour of experimental Q_{CA} as a function of total molecular density. Extrapolation to zero density by a straight line renders a value for $\log\left(Q_{CA}\right) = -2.3 \pm 0.1$.

Fig. 5

Q_{CA} as a function of total molecular density for equimolar mixtures of PA-Cy3.5-5'—PT-AF-3' of different concentration. Six different samples are plotted and identified by different symbols. The spread in the points of each sample corresponds to statistical variation in the different fields of view

From this value of Q_{CA} and according to Eq. 8 it was possible to calculate the value of $\log K_h = 7.7 \pm 0.1$, which is within uncertainty, similar to the result of the bulk experiments.

4. Discussion

The determination of a confident value for an equilibrium constant derived from counting isolated and associated molecules must be performed with great care and multiple checks. In this case, multiple counting of the same molecule was prevented by cluster analysis. The center of mass of each cluster is randomly distributed in our experiments, as expected for a spin coated solution. Cluster analysis should be performed, depending on the technique used to derive molecular localizations, also incorporating other analysis, such as for example q-PAINT, if applicable [31]. Replacement of a group of molecular localizations by the center of mass of the cluster should be

checked for consistency. For example, a random distribution might not be expected in a cell environment. In this case a simulation and check must be performed from available information on cellular location of the target molecules. Comparison to the reference value of the association derived from a random distribution of the same number of molecules in the same environment should be always performed.

The criterion to discern associated and isolated molecules depends on the critical distance chosen. This is a crucial value. In the present example, this value was taken as 100 nm, even though the average uncertainty in individual molecular localization is 40 nm. It is not surprising that the critical distance is greater than the uncertainty in individual molecular localization because of multiple counting of the same molecule, as cluster analysis shows, enlarges the region of its localization. Of course, enlarging the value of the critical distance, increases the value of the computed Q_{CA}. But this increase, though monotonous, displays two recognizable phases, as shown in Figure S4. We must take into consideration that thermodynamics measures the difference in Gibbs free energy for a process, under constant pressure and temperature. This magnitude is directly related to $\log K_h$. Thus, the value under consideration should be $\log Q_{CA}$ for the following analysis. At low values of the critical radius for considering association, there is a fast increase in the value of $\log Q_{CA}$, due to a fast incorporation of nearby partners. At high values of the critical radius, associated molecules were already completely included and the increase in $\log Q_{CA}$ is attributed to the incorporation of randomly located partners. These two regimes are depicted by the straight tendency lines in Figure S4, which cross around 100 nm. In the present case, this value is also appreciably smaller than the average distance to the first neighbour of any pair under consideration, which lies in the 500–1000 nm range.

Finally, we will discuss the range of values of an association constant that can be determined by SMLM measurements. For that, we must keep in mind that the most adequate concentration range to measure the value of an association equilibrium constant is equal to its inverse value, expressed in M units. This means that a value of 10^6 M^{-1} is best measured around micromolar concentration as the change in concentration of all three species is appreciable at the same time. Therefore, our analysis is based on the practical concentration range in which SMLM measurements can be performed.

The lower limit of concentration depends on the ability to detect a statistically significant amount of molecules. To estimate this lower limit of concentration, we will take as reference the observation volume we had in our experiments: 20 fL (500 µm^2 area of a 40-nm-thick sample). Assuming Poisson distribution for the number of molecules observed, around 1000 molecules should be detected to have a 3% statistical error. In a 1 nM solution, 1000 molecules are contained in approximately 1.7 pL. To detect this number of molecules, 85 fields of view should be added to diminish statistical noise of the distribution. Sampling a higher number of spots accepting higher statistical errors or measuring thicker samples can, of course, be considered. However, this lower limit of concentration cannot be extended much more than an order of magnitude. Therefore, we estimate the upper value of the association constant as $K_{h, max} = 10^9$ M^{-1}.

The upper limit of concentration is determined by the localization uncertainty. To estimate this limit of concentration, we will assume a maximum density of one molecule in a square area of 100 nm side. This renders 50,000 molecules in the field of view of 500 μm^2, representing a concentration of $4 \cdot 10^{-6}$ M (in a 40 nm thick sample). Under these conditions a value of $K_{h, min} = 2.5 \cdot 10^5$ M^{-1} can be adequately measured. **AQ3** In SMLM a localization uncertainty of 10 nm can be attained and consequently it is in principle possible to push down the limit of $K_{h, min}$ but, normally, the most interesting range is the opposite one of high affinities.

5. **Conclusions**

We tested a method to estimate association equilibrium constants of two partners by fluorescence SMLM that considers the multiple counting effect of the molecules, as well as the effect of incomplete labeling-detection. **AQ4** This opens the possibility to determine this parameter in cellular environments provided the volume of interaction is determined appropriately; for example, by retrieving the area occupied by the interacting species and the penetration depth of the excitation source or the membrane thickness if it is known that molecules only located in the cell membrane. **AQ5** It is worth noting that even a factor of two uncertainty in the observation volume, will only cause 0.3 error in pK. The practical limits of association constants of two partners that can be measured by SMLM is $5 \leq \log K_h \leq 9$.

Declarations

Conflict of interest   The authors have no relevant financial or non-financial interests to disclose.

Supplementary Information

Below is the link to the electronic supplementary material.

Supplementary file1 (DOCX 472 KB)

References

1. Hell, S. W. (2015). Nanoscopy with focused light (nobel lecture). *Angewandte Chemie International Edition, 54*, 8054–8066. https://doi.org/10.1002/ANIE.201504181

2. Betzig, E. (2015). Single molecules, cells, and super-resolution optics (nobel lecture). *Angewandte Chemie International Edition, 54*, 8034–8053. https://doi.org/10.1002/ANIE.201501003

3. Rust, M. J., Bates, M., & Zhuang, X. (2006). Sub-diffraction-limit imaging by stochastic optical reconstruction microscopy (STORM). *Nature Methods, 3*(10), 793–796. https://doi.org/10.1038/nmeth929

4. Bates, M., Huang, B., Rust, M. J., Dempsey, G. T., Wang, W., & Zhuang, X. (2010). Sub-diffraction-limit imaging with stochastic optical reconstruction microscopy. *Springer Series in Chemical Physics, 96*, 399–415. https://doi.org/10.1007/978-3-642-02597-6_20

5. Betzig, E., Patterson, G. H., Sougrat, R., Lindwasser, O. W., Olenych, S., Bonifacino, J. S., Davidson, M. W., Lippincott-Schwartz, J., & Hess, H. F. (2006). Imaging intracellular fluorescent proteins at nanometer resolution. *Science, 313*, 1642–1645. https://doi.org/10.1126/SCIENCE.1127344

6. Hummert, J., Tashev, S. A., & Herten, D. P. (2021). An update on molecular counting in fluorescence microscopy. *The International Journal of Biochemistry & Cell Biology, 135*, 105978. https://doi.org/10.1016/J.BIOCEL.2021.105978

7. Nicovich, P. R., Owen, D. M., & Gaus, K. (2017). Turning single-molecule localization microscopy into a quantitative bioanalytical tool. *Nature Protocols, 12*(3), 453–460. https://doi.org/10.1038/nprot.2016.166

8. Sharonov, A., & Hochstrasser, R. M. (2006). Wide-field subdiffraction imaging by accumulated binding of diffusing probes. *Proceedings of the National Academy of Sciences, 103*, 18911–18916. https://doi.org/10.1073/PNAS.0609643104

9. Khater, I. M., Nabi, I. R., & Hamarneh, G. (2020). A review of super-resolution single-molecule localization microscopy cluster analysis and quantification methods. *Patterns, 1*, 100038. https://doi.org/10.1016/j.patter.2020.100038

10. Szalai, A. M., Armando, N. G., Barabas, F. M., Stefani, F. D., Giordano, L., Bari, S. E., Cavasotto, C. N., Silberstein, S., & Aramendía, P. F. (2018). A fluorescence nanoscopy marker for corticotropin-releasing hormone type 1 receptor: Computer design, synthesis, signaling effects, super-resolved fluorescence imaging, and in situ affinity constant in cells. *Physical Chemistry Chemical Physics, 20*, 29212–29220. https://doi.org/10.1039/C8CP06196C

11. Dunn, K. W., Kamocka, M. M., & Mcdonald, J. H. (2011). A practical guide to evaluating colocalization in biological microscopy. *American Journal of Physiology. Cell Physiology, 300*, 723–742. https://doi.org/10.1152/ajpcell.00462.2010

12. Schermelleh, L., Ferrand, A., Huser, T., Eggeling, C., Sauer, M., Biehlmaier, O., & Drummen, G. P. C. (2019). Super-resolution microscopy demystified. *Nature Cell Biology, 21*(1), 72–84. https://doi.org/10.1038/s41556-018-0251-8

13. Dietz, M. S., & Heilemann, M. (2019). Optical super-resolution microscopy unravels the molecular composition of functional protein complexes. *Nanoscale, 11*, 17981–17991. https://doi.org/10.1039/C9NR06364A

14. Annibale, P., Vanni, S., Scarselli, M., Rothlisberger, U., & Radenovic, A. (2011). Quantitative photo activated localization microscopy: unraveling the effects of photoblinking. *PLoS ONE, 6*, 22678. https://doi.org/10.1371/journal.pone.0022678

15. Dempsey, G. T., Vaughan, J. C., Chen, K. H., Bates, M., & Zhuang, X. (2011). Evaluation of fluorophores for optimal performance in localization-based super-resolution imaging. *Nature Methods, 8*(12), 1027–1036. https://doi.org/10.1038/nmeth.1768

16. Lelek, M., Gyparaki, M. T., Beliu, G., Schueder, F., Griffié, J., Manley, S., Jungmann, R., Sauer, M., Lakadamyali, M., & Zimmer, C. (2021). Single-molecule localization microscopy. *Nature Reviews Methods Primers, 1*(1), 1–27. https://doi.org/10.1038/s43586-021-00038-x

17. Baumgart, F., Arnold, A. M., Leskovar, K., Staszek, K., Fölser, M., Weghuber, J., Stockinger, H., & Schütz, G. J. (2016). Varying label density allows artifact-free analysis of membrane-protein nanoclusters. *Nature Methods, 13*(8), 661–664. https://doi.org/10.1038/nmeth.3897

18. Sengupta, P., Jovanovic-Talisman, T., & Lippincott-Schwartz, J. (2013). Quantifying spatial organization in point-localization superresolution images using pair correlation analysis. *Nature Protocols, 8*(2), 345–354. https://doi.org/10.1038/nprot.2013.005

19. Owczarzy, R., Huang, L., Manthey, J. A., Mcquisten, K. A., Behlke, M. A., & Walder, J. A. (2002). Thermodynamic treatment of oligonucleotide duplex-simplex equilibria. *Biophysical Journal, 82*, 30. https://doi.org/10.1073/pnas.2335948100

20. Mathur, D., Samanta, A., Ancona, M. G., Díaz, S. A., Kim, Y., Melinger, J. S., Goldman, E. R., Sadowski, J. P., Ong, L. L., Yin, P., & Medintz, I. L. (2021). Understanding Förster resonance energy transfer in the sheet regime with DNA brick-based dye networks. *ACS Nano, 15*, 16452–16468. https://doi.org/10.1021/acsnano.1c05871

21. Sanborn, M. E., Connolly, B. K., Gurunathan, K., & Levitus, M. (2007). Fluorescence properties and photophysics of the sulfoindo cyanine Cy3 linked covalently to DNA. *The Journal of Physical Chemistry B, 111*(37), 11064-11074. https://doi.org/10.1021/jp072 912u

22. Kibbe, W. A. (2007). OligoCalc: An online oligonucleotide properties calculator. *Nucleic Acids Research, 35*, W43–W46. https://doi.org/10.1093/NAR/GKM234

23. Bielec, K., Sozanski, K., Seynen, M., Dziekan, Z., Ten Wolde, P. R., & Holyst, R. (2019). Kinetics and equilibrium constants of oligonucleotides at low concentrations. Hybridization and melting study. *Physical Chemistry Chemical Physics, 21*, 10798–10807. https://doi.org/10.1039/C9CP01295H

24. Bielec, K., Bubak, G., Kalwarczyk, T., & Holyst, R. (2020). Analysis of brightness of a single fluorophore for quantitative characterization of biochemical reactions. *Journal of Physical Chemistry B, 124*, 1941–1948. https://doi.org/10.1021/acs.jpcb.0c00770

25. Hall, D. B., Underhill, P., & Torkelson, J. M. (1998). Spin coating of thin and ultrathin polymer films. *Polymer Engineering & Science, 38*, 2039–2045. https://doi.org/10.1002/PEN.10373

26. Ester, M., Kriegel, H.-P., Sander, J., & Xu, X. (1996). A density-based algorithm for discovering clusters in large spatial databases with noise. *KDD-96 Proceedings* , 226–231.

27. Mazouchi, A., Milstein, J. N. (2016). Fast optimized cluster algorithm for localizations (FOCAL): a spatial cluster analysis for super-resolved microscopy. *Bioinformatics*. *32*(5), 747-754. https://doi.org/10.1093/bioinformatics/btv630

28. Joshi, P., & Mondal, P. P. (2021). Single-molecule clustering for super-resolution optical fluorescence microscopy. *Photonics, 2022*(9), 7. https://doi.org/10.3390/PHOTONICS9010007

29. Hellriegel, C., Kirstein, J., Bräuchle, C., Latour, V., Pigot, T., Olivier, R., Lacombe, S., Brown, R., Guieu, V., Payrastre, C., Izquierdo, A., & Mocho, P. (2004). Diffusion of single streptocyanine molecules in the nanoporous network of sol-gel glasses. *Journal of Physical Chemistry B, 108*, 14699–14709. https://doi.org/10.1021/JP049412A

30. Szalai, A. M., Lopez, L. F., Morales-Vásquez, M. Á., Stefani, F. D., & Aramendía, P. F. (2020). Analysis of sparse molecular distributions in fibrous arrangements based on the distance to the first neighbor in single molecule localization microscopy. *Nanoscale, 12*, 9495–9506. https://doi.org/10.1039/c9nr10805j

31. Jungmann, R., Avendaño, M. S., Dai, M., Woehrstein, J. B., Agasti, S. S., Feiger, Z., Rodal, A., & Yin, P. (2016). Quantitative super-resolution imaging with qPAINT. *Nature Methods, 13*, 439–442. https://doi.org/10.1038/nmeth.3804